Expanded View Figures

Figure EV1. Characterisation of RPE-1 CyclinB1-mEmerald$^{+/+}$ and APC8-mScarlet$^{+/+}$ cells.

(**A**) Representative fluorescence confocal image of RPE-1 CyclinB1-mEmerald$^{+/+}$; APC8$^{+/+}$ cells in interphase. The scale bar corresponds to 20 µm. (**B**) Representative fluorescence confocal images over time of a CyclinB1-mEmerald$^{+/+}$; APC8$^{+/+}$ cell progressing through mitosis. Time is expressed as mm:ss. The scale bar corresponds to 10 µm. (**C**) Dot plots of the mitotic timing of parental RPE-1, RPE-1 APC8-mScarlet$^{+/+}$, RPE-1 CyclinB1-mEmerald$^{+/+}$ and APC8-mScarlet$^{+/+}$ cells, untreated (left) or treated with 100 nM paclitaxel (right). Each small dot represents one cell and large dots represent the median of independent experiments: $n \geq 83$ cells per condition, $N = 3$ independent experiments. Numbers on the graphs indicate the percentage of cells completing mitosis during the time of observation. Clones marked in red are the ones selected for all following experiments. (**D**) Top, growth curve of RPE-1 (black), RPE-1 APC8-mScarlet$^{+/+}$(orange), RPE-1 CyclinB1-mEmerald$^{+/+}$ and APC8-mScarlet$^{+/+}$(red), $N = 3$ experiment. Mean ± standard deviation are plotted. Bottom, dot plot of the chromosome number of parental RPE-1, RPE-1 APC8-mScarlet$^{+/+}$, RPE-1 CyclinB1-mEmerald$^{+/+}$ and APC8-mScarlet$^{+/+}$ cells. Each dot represents one chromosome spread: $n \geq 34$ spreads per condition, $N = 2$. (**E**) Representative anti-APC8, anti-APC4 and β-Tubulin immunoblot of cell lysates from parental RPE-1, RPE-1 APC8-mScarlet$^{+/+}$, RPE-1 CyclinB1-mEmerald$^{+/+}$ and APC8-mScarlet$^{+/+}$ cells before and after immunodepleting APC4, compared with control immunodepletion with IgG. (**F**) Bar graphs representing the quantification of the immunoblot in (panel **E**). $N = 2$ independent experiments. Mean ± standard deviation are plotted. (**G**) Graph representing the autocorrelation function of APC8-mScarlet over time in the nucleus. (**H**) Quantification of normalised Cyclin B1 fluorescence levels over time measured by spinning-disk fluorescence microscopy in RPE-1 CyclinB1-mEmerald$^{+/+}$ cells compared to RPE-1 CyclinB1-mEmerald$^{+/+}$; RPE-1 APC8-mScarlet$^{+/+}$, RPE-1 CyclinB1-mEmerald$^{+/+}$ cells. $n \geq 9$ cells per condition, $N = 3$ independent experiments. Mean ± standard deviation are plotted. Figure EV1 – Supplementary text to determine whether APC8-mScarlet is properly incorporated into the APC/C, we reasoned that immunoprecipitating an APC/C subunit would result in a depletion of APC8 levels in the lysate. Measuring the levels of APC8 immunodepletion following immunoprecipitation of APC4 revealed no significant cgq RPE-1, RPE APC8-mScarlet$^{+/+}$, and RPE APC8-mScarlet$^{+/+}$; Cyclin B1-mEmerald$^{+/+}$ cells, indicating that mScarlet does not interfere with APC8 incorporation into the APC/C.

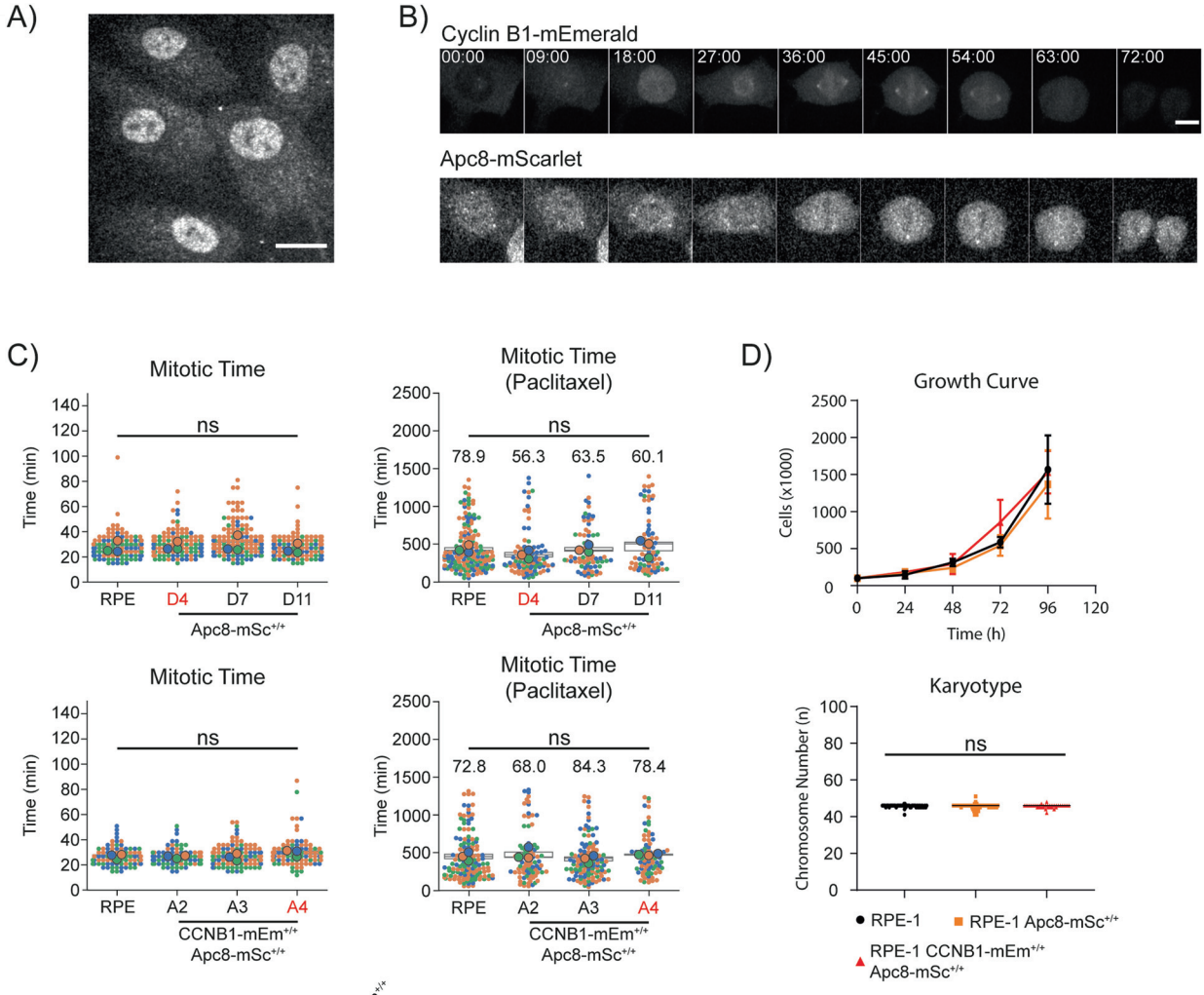
A)
B)
Cyclin B1-mEmerald
00:00
09:00
18:00
27:00
36:00
45:00
54:00
63:00
72:00
Apc8-mScarlet
C)
Mitotic Time
Time (min)
ns
RPE
D4
D7
D11
Apc8-mSc+/+
Mitotic Time (Paclitaxel)
78.9
56.3
63.5
60.1
Mitotic Time
RPE
A2
A3
A4
CCNB1-mEm+/+
Apc8-mSc+/+
Mitotic Time (Paclitaxel)
72.8
68.0
84.3
78.4
D)
Growth Curve
Cells (x1000)
Time (h)
Karyotype
Chromosome Number (n)
RPE-1
RPE-1 Apc8-mSc+/+
RPE-1 CCNB1-mEm+/+
Apc8-mSc+/+
E)
Parental
Apc8-mSc+/+
CCNB1-mEm+/+
Apc8-mSc+/+
KDa
Apc4
Apc8 -mScarlet
Apc8
β-Tub
100
75
50
Input
ID Apc4
ID IgG
F)
Apc8 Levels (Apc4 ID)
Apc8 Levels (Input)
Apc4 Levels (Input)
Normalized Fluorescence Intensity
***
RPE-1
RPE-1 Apc8-mSc+/+
RPE-1 CCNB1-mEm+/+ Apc8-mSc+/+
G)
Apc8-mScarlet Autocorrelation (Nucleus)
G(t) - Nucleus
Apc8-mSc (Data)
Apc8-mSc (Fit)
Lag time (ms)
H)
Cyclin B1 - mEmerald Fluorescence Intensity
Normalized RID
Time (min)
RPE-1 CCNB1-mEm+/+
RPE-1 CCNB1-mEm+/+ Apc8-mSc+/+

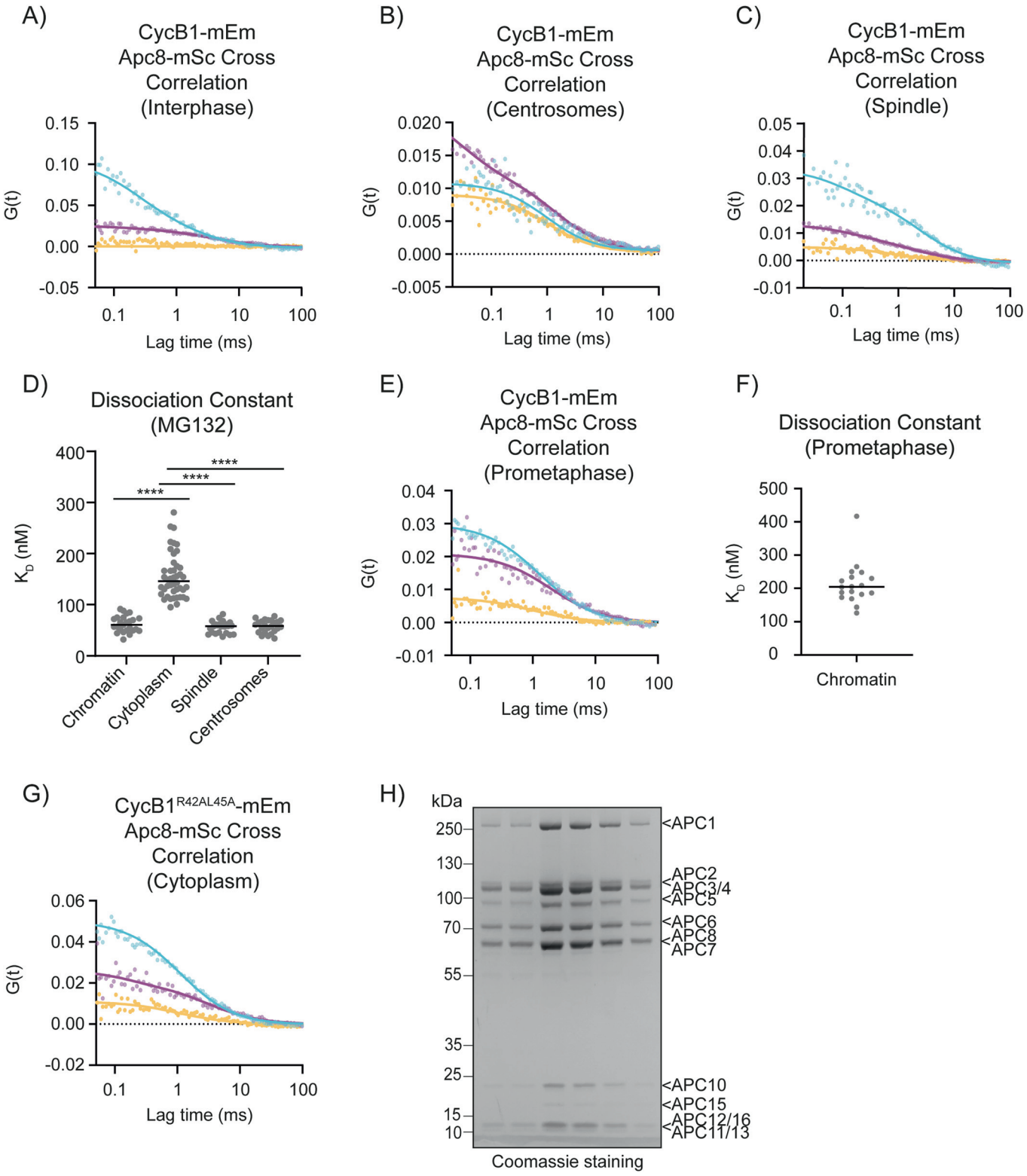

Figure EV2. FCCS of Cyclin B1-mEmerald and APC8-mScarlet.

(**A–C**, **E**, **G**) Representative graphs of the autocorrelation function of mEmerald and mScarlet and the cross-correlation function between the two in RPE-1 CyclinB1-mEmerald$^{+/+}$; APC8-mScarlet$^{+/+}$ (**A–C**, **E**), and in RPE-1 APC8-mScarlet$^{+/+}$ cells ectopically expressing Cyclin B1^{R45AL45A}-mEmerald (**G**). (**D**, **F**) Dot plots representing the K_D between endogenous Cyclin B1-mEmerald and APC8-mScarlet in metaphase cells following MG132 treatment (**D**) or in untreated prometaphase cells (**F**). $n \geq 18$ cells per condition, $N = 3$ independent experiments. (**H**) Fractions from a ResourceQ elution of the APC/C purification. Run on a 4–12% Bis-Tris SDS-PAGE gel.

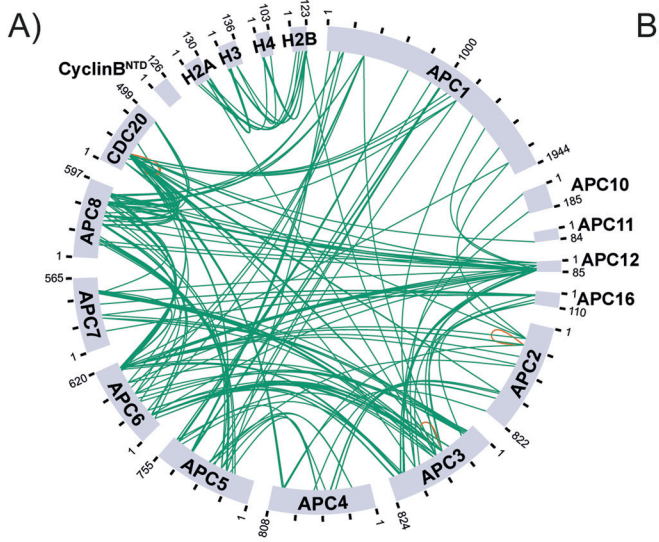
A)
CyclinB^NTD
H2A
H3
H4
H2B
APC1
APC10
APC11
APC12
APC16
APC2
APC3
APC4
APC5
APC6
APC7
APC8
CDC20

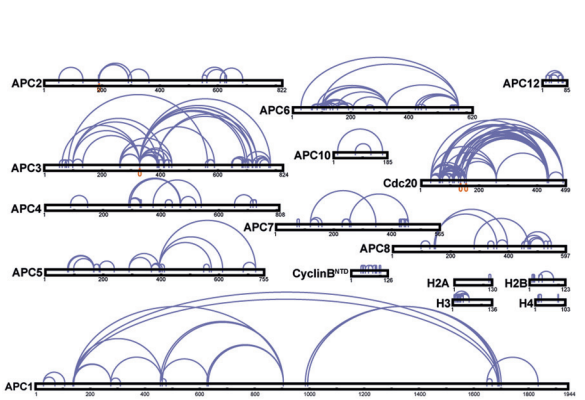
B)
APC2
APC6
APC12
APC3
APC10
Cdc20
APC4
APC7
APC8
APC5
CyclinB^NTD
H2A
H2B
H3
H4
APC1

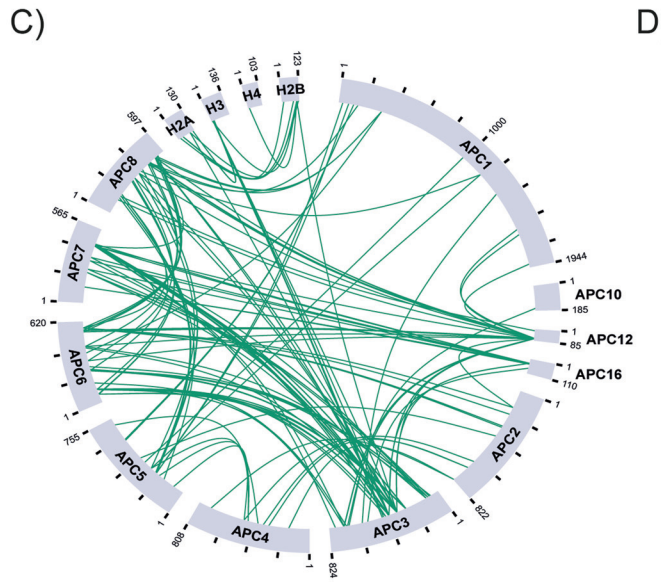
C)
H2A
H3
H4
H2B
APC1
APC10
APC12
APC16
APC2
APC3
APC4
APC5
APC6
APC7
APC8

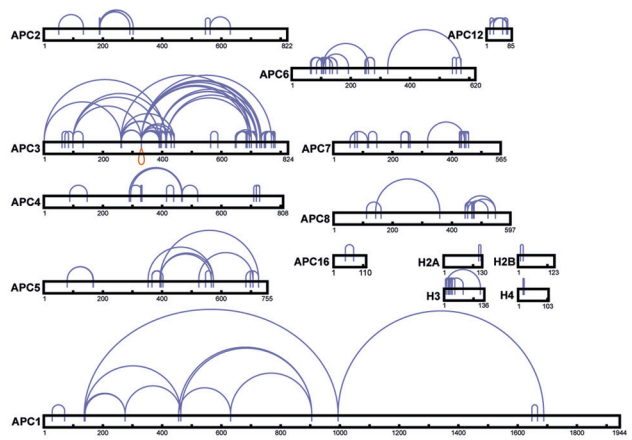
D)
APC2
APC12
APC6
APC3
APC7
APC4
APC8
APC16
H2A
H2B
APC5
H3
H4
APC1

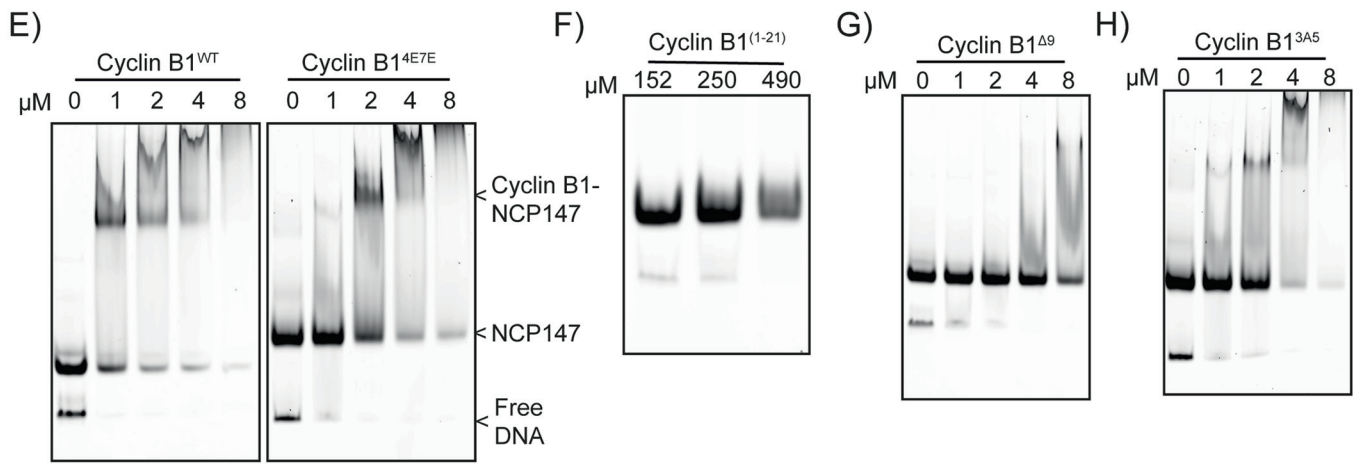
E)
Cyclin B1^WT
Cyclin B1^4E7E
μM 0 1 2 4 8
0 1 2 4 8
Cyclin B1-NCP147
NCP147
Free DNA
F)
Cyclin B1^(1-21)
μM 152 250 490
G)
Cyclin B1^Δ9
μM 0 1 2 4 8
H)
Cyclin B1^3A5
μM 0 1 2 4 8

Figure EV3. Cyclin B1 binding to nucleosomes.

(**A**) Representation of heteromeric crosslinks of the APC/C-CDC20-Cyclin $B1^{NTD}$ complex with the NCP. (**B**) Representation of the self-crosslinks of individual APC/C subunits, CDC20, Cyclin $B1^{NTD}$ and the four histones. (**C**) Representation of heteromeric crosslinks of the APC/C with the NCP. (**D**) Representation of self-crosslinks of individual APC/C subunits and histones. (**E–H**). EMSA of NCP147 with the indicated variant of Cyclin B1. $N = 3$ independent experiments.

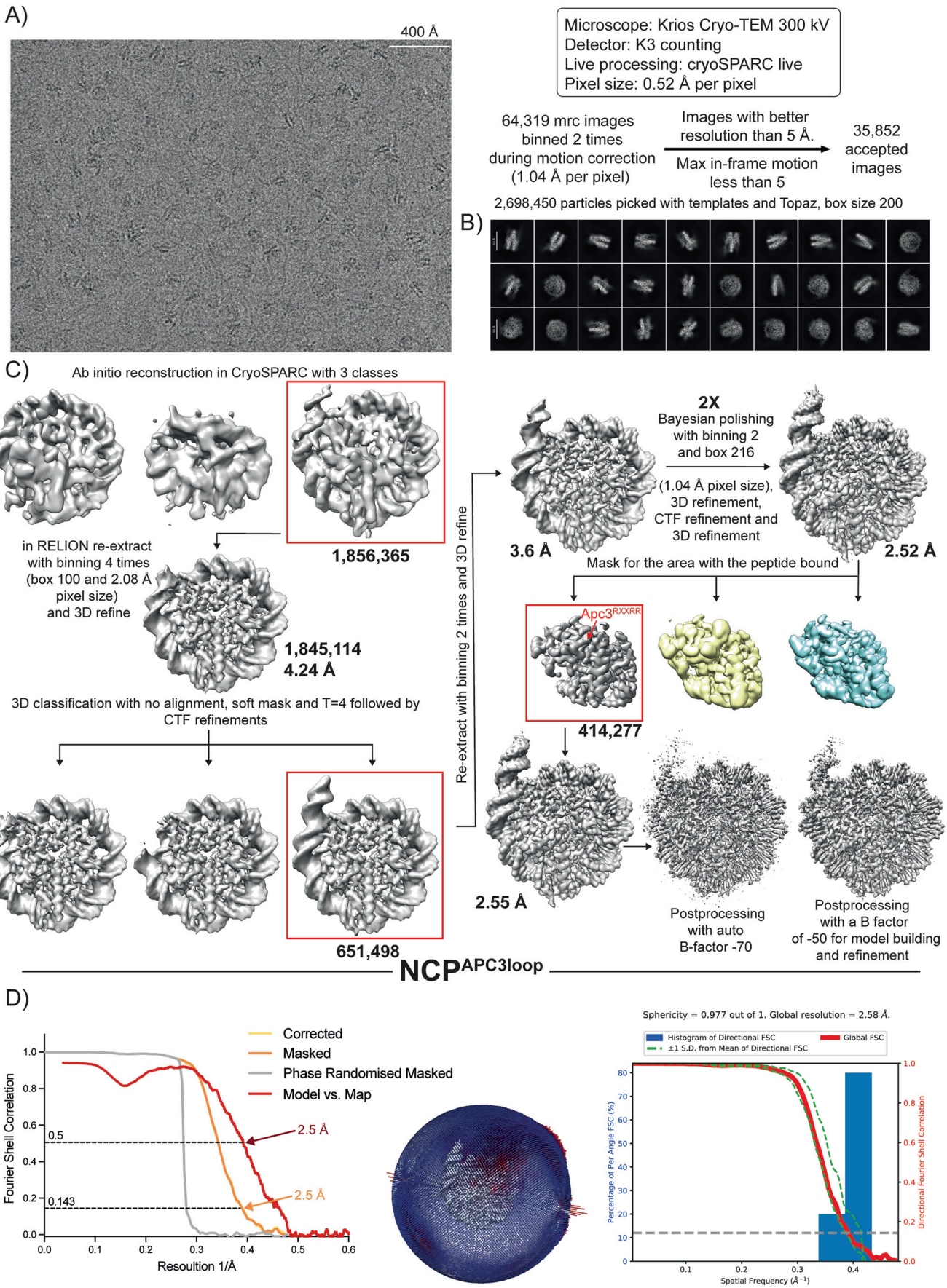
A)
400 Å
Microscope: Krios Cryo-TEM 300 kV
Detector: K3 counting
Live processing: cryoSPARC live
Pixel size: 0.52 Å per pixel
64,319 mrc images
binned 2 times
during motion correction
(1.04 Å per pixel)
Images with better
resolution than 5 Å.
Max in-frame motion
less than 5
35,852
accepted
images
2,698,450 particles picked with templates and Topaz, box size 200
B)
C)
Ab initio reconstruction in CryoSPARC with 3 classes
1,856,365
in RELION re-extract
with binning 4 times
(box 100 and 2.08 Å
pixel size)
and 3D refine
1,845,114
4.24 Å
3D classification with no alignment, soft mask and T=4 followed by
CTF refinements
651,498
2X
Bayesian polishing
with binning 2
and box 216
(1.04 Å pixel size),
3D refinement,
CTF refinement and
3D refinement
3.6 Å
2.52 Å
Mask for the area with the peptide bound
Apc3RXXRR
414,277
Re-extract with binning 2 times and 3D refine
2.55 Å
Postprocessing
with auto
B-factor -70
Postprocessing
with a B factor
of -50 for model building
and refinement
NCPAPC3loop
D)
Corrected
Masked
Phase Randomised Masked
Model vs. Map
Fourier Shell Correlation
Resoultion 1/Å
0.5
0.143
2.5 Å
2.5 Å
Sphericity = 0.977 out of 1. Global resolution = 2.58 Å.
Histogram of Directional FSC
Global FSC
±1 S.D. from Mean of Directional FSC
Percentage of Per Angle FSC (%)
Directional Fourier Shell Correlation
Spatial Frequency (Å⁻¹)

Figure EV4. Cryo-EM analysis of the nucleosome core particle in complex with APC3 loop$^{177-446}$.

(**A–C**) Workflow showing a representative micrograph, the cryo-EM data collection parameters (**A**) and the single-particle analysis pipeline for the nucleosome core particle with the APC3 loop$^{177-446}$ (**B**, **C**). N. of particles at each classification step is indicated. (**D**) Fourier shell correlation (FSC) curves, angular distribution plot and plot of the directional FSC that represent a measure of directional resolution anisotropy for all the reconstructions are shown. Directional FSC and sphericity determination was performed with the 3DFSC software (Tan et al, 2017).

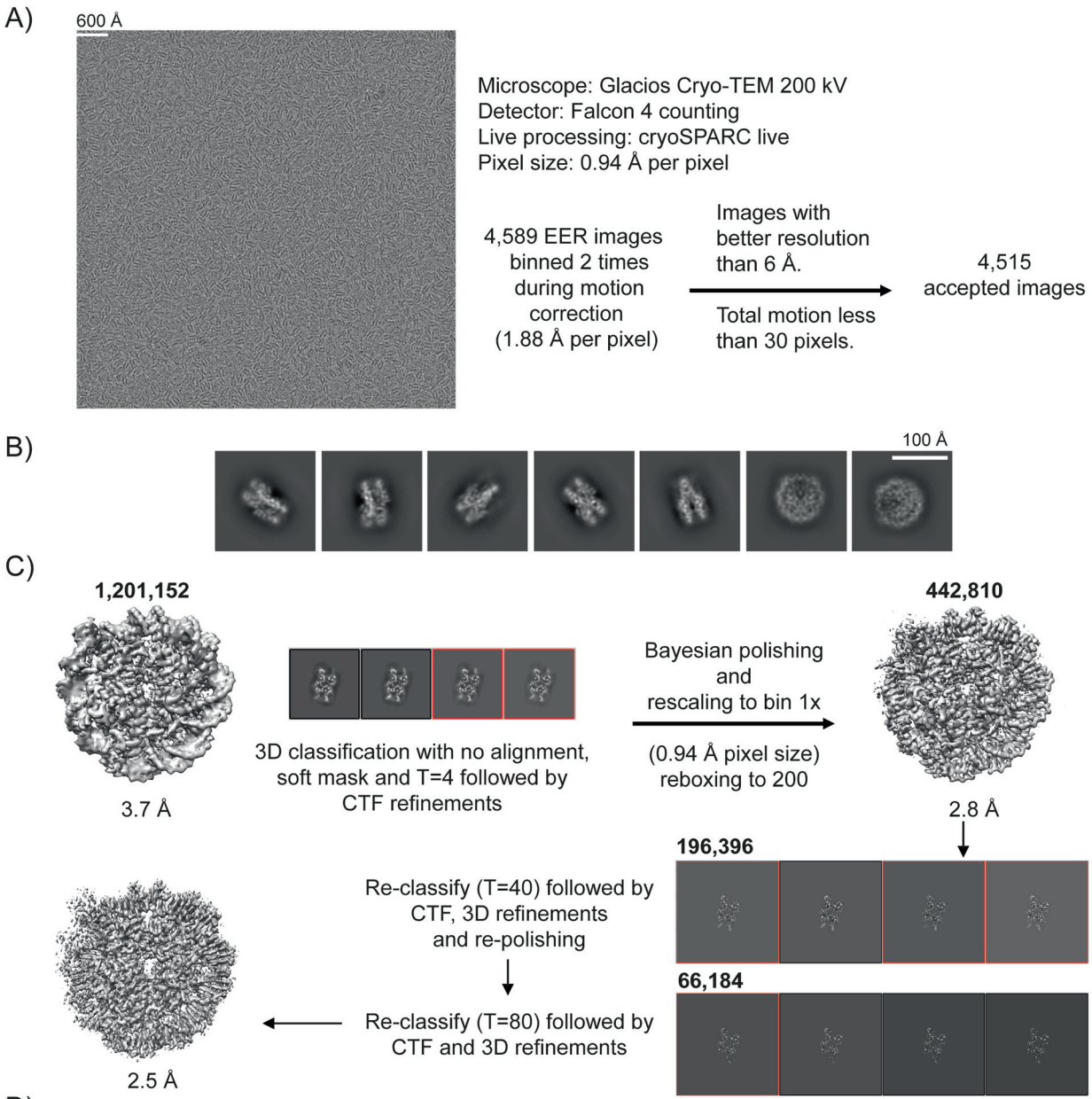
A)
600 Å
Microscope: Glacios Cryo-TEM 200 kV
Detector: Falcon 4 counting
Live processing: cryoSPARC live
Pixel size: 0.94 Å per pixel
4,589 EER images binned 2 times during motion correction (1.88 Å per pixel)
Images with better resolution than 6 Å.
Total motion less than 30 pixels.
4,515 accepted images
B)
100 Å
C)
1,201,152
3.7 Å
3D classification with no alignment, soft mask and T=4 followed by CTF refinements
Bayesian polishing and rescaling to bin 1x
(0.94 Å pixel size) reboxing to 200
442,810
2.8 Å
196,396
66,184
Re-classify (T=40) followed by CTF, 3D refinements and re-polishing
Re-classify (T=80) followed by CTF and 3D refinements
2.5 Å
D)
NCPCbNT
Corrected
Masked
Phase Randomised Masked
Model vs. Map
Fourier Shell Correlation
Resoultion 1/Å
0.5
0.143
2.7 Å
2.5 Å
Sphericity = 0.960 out of 1. Global resolution = 2.59 Å.
Histogram of Directional FSC
±1 S.D. from Mean of Directional FSC
Global FSC
Percentage of Per Angle FSC (%)
Directional Fourier Shell Correlation
Spatial Frequency (Å⁻¹)

Figure EV5. Cryo-EM analysis of the nucleosome core particle in complex with Cyclin B1 N-terminus.

(**A–C**) Workflow showing a representative micrograph, the cryo-EM data collection parameters (**A**) and the single-particle analysis pipeline for the nucleosome core particle in complex with Cyclin B N-terminus (NCP^{CbNT}) (**B**, **C**). N. of particles at each classification step is indicated. (**D**) Fourier shell correlation (FSC) curves, angular distribution plot and plot of the directional FSC that represent a measure of directional resolution anisotropy for all the reconstructions are shown. Directional FSC and sphericity determination was performed with the 3DFSC software.